

Dynamic Measurements of Laser Light Attenuation by Cryogen Film and Frost Formation

Bernard Choi^{1,2}, Guillermo Aguilar^{1,3}, Gracie Vargas², A.J. Welch², and J. Stuart Nelson^{1,3}

¹Beckman Laser Institute and Medical Clinic, University of California, Irvine, CA 92612

²Department of Biomedical Engineering, The University of Texas, Austin, TX 78712

³Whitaker Center for Biomedical Engineering, University of California, Irvine, CA 92612

ABSTRACT

The purpose of this study was to investigate the dynamics of laser light attenuation during cryogen spray cooling (CSC). Two detection schemes were used to approximate collimated and diffuse light transmittance measurements of continuous-wave ($\lambda = 594$ nm) and pulsed ($\lambda = 585$ nm) laser light during application of short (20-100 ms duration) cryogen spurts on a glass substrate. High-speed video images were also obtained during CSC. Collimated light transmittance varied considerably during CSC. Comparison of collimated and total transmitted light detection indicated that the diffuse component was substantial. Light attenuation occurred despite transparency of the liquid cryogen layer. Light scattering by cryogen results in a diverging laser beam incident on the skin surface. Since specular reflectance at the cryogen-skin interface may differ for diffuse light, further study of light scattering during CSC is warranted. Due to the differences in optical properties of glass and skin, experiments on skin need to be performed to extrapolate our results to the clinical scenario. For dermatologic procedures such as laser port wine stain and vascular lesion removal, hair removal, and nonablative skin rejuvenation, recommended τ_d are 10-80 ms. This range of τ_d appears to be appropriate, although more studies are required to arrive at a definite conclusion.

Keywords: cryogen spray cooling, port wine stains, transmittance, dermatology, skin

1. INTRODUCTION

Cryogen spray cooling (CSC) is a technique used to precool skin during laser therapy. The selective cooling provided by CSC spatially confines reduced temperatures to the epidermis, which counteracts unwanted epidermal heating by the ensuing laser pulse. CSC is used clinically during laser-mediated dermatological procedures such as treatment of port wine stains (PWS) [1-6] and hemangiomas [7-9], hair removal [10], and nonablative skin rejuvenation [11, 12]

During CSC, atomized cryogen droplets propagate from the delivery nozzle to the skin surface. Initial droplets reach the skin surface and rapidly remove heat from the skin. At later stages of the spurt, the rate of droplet deposition may exceed the rate at which the droplets evaporate, resulting in formation of a liquid cryogen pool on the skin surface. The cryogen pool eventually evaporates as frost forms on the skin surface due to condensation of water vapor present in the local environment.

Thus, CSC is characterized by a dynamic surface boundary condition. Previous studies have established that incident laser light is attenuated during CSC. Anvari et al. [2] sprayed cryogen on the surface of dry collagen films and measured an 85-90% transmittance of 585-nm laser light. Majaron et al. [13] sprayed a 2-s cryogen spurt into a glass cup and measured 80% transmittance of pulsed Er:YAG ($\lambda = 2.94$ μm) laser radiation. Pope and MacKenzie [14] measured >97% transmittance of pulsed 755-nm laser light during CSC of glass. A limitation of these reported transmittances is that information on the relative timing of these measurements with respect to the cryogen spurt is not provided.

The purpose of this study was to investigate laser light attenuation by the cryogen film/frost layer. Medical-grade, FDA-approved cryogen was sprayed on a glass slide, and continuous-wave (CW) and pulsed laser light transmittance during CSC was measured. High-speed video images during CSC were obtained and correlated with the time-resolved transmittance measurements.

2. MATERIALS AND METHODS

2.1. Basic Experimental Setup

A commercial cryogen delivery system (Dynamic Cooling Device (DCD), Candela Corporation, Wayland, MA) was used in all experiments. The test cryogen was refrigerant R134a (-26°C boiling point temperature at 1 atm) and is the cryogen currently used in clinical laser PWS and hemangioma treatments [1-3, 6, 7, 9, 15]. The DCD was triggered using a relay switch controlled by a digital pulse generator (Model DG535, Stanford Research Systems, Sunnyvale, CA).

Cryogen spurts of 20-, 60-, and 100-ms durations (τ_{cry}) were delivered to one surface of a 1-mm-thick glass slide. The distance between the DCD handpiece nozzle exit and glass slide was approximately 5 cm and was kept constant for all experiments. Since laser light was incident normal to the glass slide surface (see below), the cryogen was delivered at a $15\text{-}30^{\circ}$ angle with respect to the normal. After each cryogen spurt, the glass slide surface was wiped with methanol-soaked lens-cleaning tissue to remove dry cryogen residue. Following each cryogen spurt, sufficient time was provided for the slide temperature to return to ambient temperature.

2.2. High-Speed Image Acquisition

Images of cryogen spurts sprayed on glass were acquired with a high-speed CCD-based imaging system (Fast-Cam Super 10K, Photron USA, San Jose, CA). The camera was oriented normal to the glass surface. The frame acquisition rate was 1000 frames per second (fps), corresponding to a pixel window size of 256×240 . Additional lighting was provided by a fiber-optic illuminator (FO-150, Chiu Technical Corporation, Kings Park, NY). Image sequences were stored on a mini-DV tape with a dedicated recording unit (Video Walkman GV-D900 NTSC, Sony, Tokyo, Japan). A total of 5000 images were captured per cryogen spurt.

2.3. CW Laser Light Detection

A HeNe laser ($\lambda = 594\text{ nm}$, Model 1677, Uniphase, Manteca, CA) served as the CW light source. Emitted laser light was attenuated by two linear polarizers (Model 069-0120, OptoSigma, Santa Ana, CA) mounted on rotational translation stages. The power incident on the glass slide was $\sim 17\text{ }\mu\text{W}$. The beam profile was gaussian with a $1/e^2$ spot diameter of 3 mm measured using the knife-edge technique [16].

A silicon photodiode (Model 818-SL, Newport Corp., Irvine, CA) detected the transmitted laser light. An iris aperture set at a 1-mm-diameter opening was mounted to the photodiode. The distance d between the front surface of the glass slide and the photodiode surface was set at 2.5, 17.5, and 32.5 cm. The aperture was used to reduce the amount of detected diffuse light and thus offer an approximation of collimated light transmittance (T). This approximation was more valid as d was increased.

The voltage output of the photodiode was acquired with a connector block (Model BNC-2110, National Instruments, Austin, TX) connected to a data acquisition board (Model PCI-MIO-16E-4, National Instruments). Software written in LabVIEW (Version 5.1, National Instruments) was used to control the timing between CSC and data acquisition.

In the experiment, a cryogen spurt was delivered to the glass slide surface. Laser light transmission was monitored prior to, during, and after CSC, for a total of 20 seconds. In this paper, the initial one-second periods will be discussed only. Five measurements were taken at each slide-detector separation and for each τ_{cry} .

2.4. Pulsed Laser Light Detection

A clinical pulsed-dye laser system (Model SPTL-1b, Candela Corporation) equipped with a DCD was used in this study. The laser emitted 450- μ s-long pulses at a wavelength of 585 nm. The radiant exposure incident on the glass slide was 3.5 J/cm². Cryogen was sprayed on the glass slide prior to pulsed laser irradiation. The delay time (τ_d) between the end of the cryogen spurt and the onset of the laser pulse was varied ($\tau_d = 10, 50, 100, \text{ and } 500 \text{ ms}$).

Incident laser light was detected using a joulemeter (Model J25-LP-1, Molectron Detector Inc., Portland, OR) connected to an energy meter (Energy Max 500, Molectron Detector Inc.). The detector was placed at two distances d away from the glass slide (4.7 and 17.5 cm) and measurements were taken with and without a 1-mm-diameter aperture placed in front of the detector. For convenience, the presence or absence of the aperture in front of the detector will be hereafter referred to as “apertured” and “nonapertured” detection, respectively.

Energy measurements were taken before (Q_{\max}) and at a time τ_d after CSC (Q_{CSC}). Transmittance T [%] was calculated by the ratio Q_{CSC}/Q_{\max} . At least three measurements were taken for each experimental condition. All data is reported as mean \pm standard deviation.

3. RESULTS

3.1. High-Speed Image Acquisition

Figure 1 shows a montage of images acquired during a 100-ms cryogen spurt at 1000 fps. A typical sequence of dynamic events occurring during and after a cryogen spurt includes the following. A pool of cryogen liquid droplets formed on the surface of the glass slide, followed by frost formation in the periphery of the pool (Figure 1, $t = 150\text{-}200 \text{ ms}$). As boiling ceased in more central regions of the sprayed area, frost formed progressively closer to the center of the sprayed area ($t = 500 \text{ ms}$) until a continuous layer of frost was present on the surface ($t = 1076 \text{ ms}$). Eventually, the frost melted, beginning at the periphery (images not shown).

From the acquired image sequences, a characteristic time τ_{cfl} was quantified, representing the time between the beginning of the cryogen spurt and the timepoint at which a continuous frost layer was present. Our initial hypothesis was that at $t = \tau_{\text{cfl}}$, light transmittance would be at a local minimum. Mean values are summarized in Table 1.

3.1. CW Laser Light Detection

Figure 2 shows plots of collimated 594-nm laser light transmittance T_c as a function of time for $\tau_{\text{cry}} = 20\text{-}, 60\text{-}, \text{ and } 100\text{-ms}$, respectively. The light transmittance changed considerably over the initial one-second interval. For $\tau_{\text{cry}} = 20 \text{ ms}$, an increase in slide-detector separation d resulted in an increased duration during which $T_c < 100\%$. For all three d , T_c eventually reached $\sim 100\%$. The trends were different for longer cryogen spurts. For $d = 2.5 \text{ cm}$, T_c eventually reached $\sim 100\%$. However, for longer d , T_c remained below 100% during the same period. Furthermore, the 60- and 100-ms transmittance curves measured for $d = 17.5$ and 32.5 cm were similar in shape, with $T_c(d = 17.5 \text{ cm})$ consistently greater than $T_c(d = 32.5 \text{ cm})$.

3.2. Pulsed Laser Light Detection

585-nm pulsed laser light transmittances are plotted in Figure 3 for select values of τ_d and for two d . $T(d = 4.7 \text{ cm})$ was greater than $T(d = 17.5 \text{ cm})$ for all τ_{cry} and τ_d . Also, T was lower in apertured detector measurements for all τ_{cry} and τ_d .

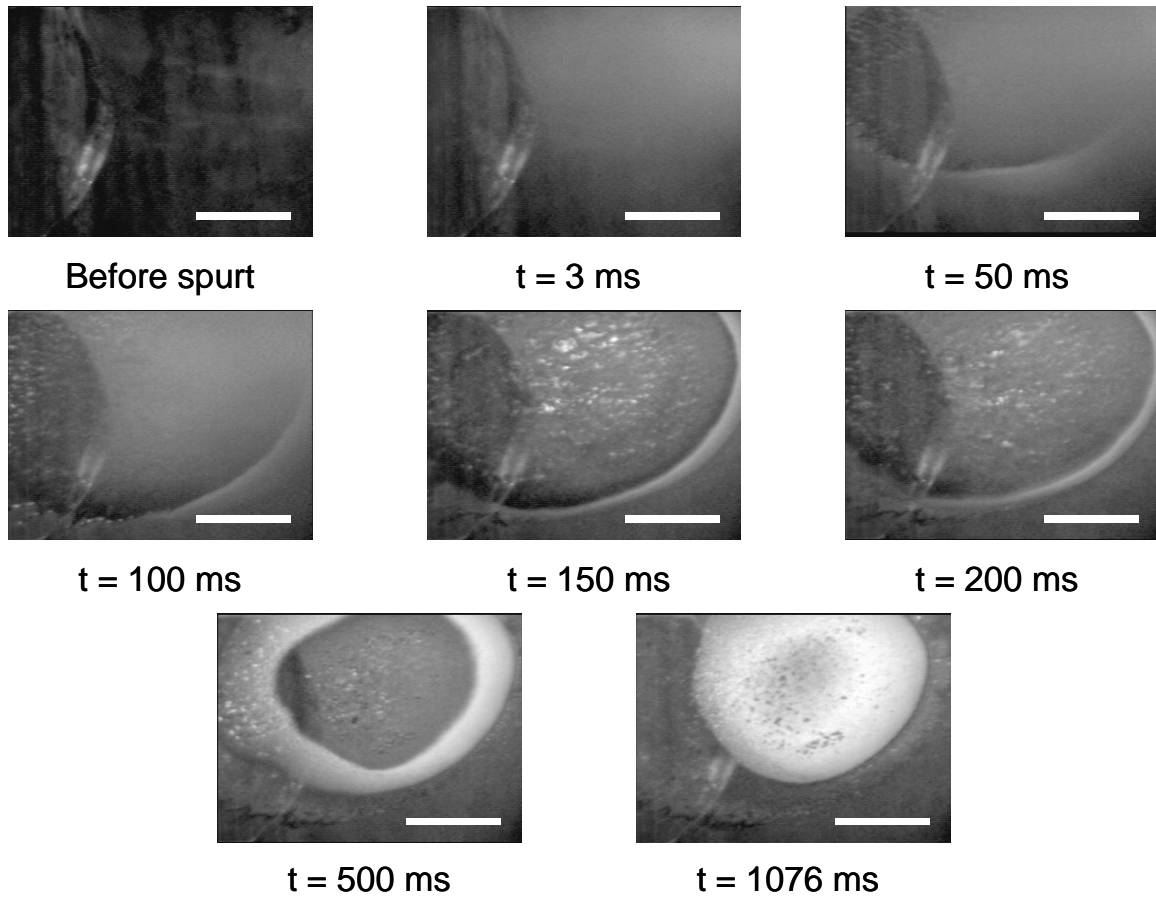


Figure 1. High-speed video image sequence obtained during CSC of glass. The cryogen spurt duration was 100 ms. The curved object on the left side of the image is a reflection of a nearby object. The images shown for $t \leq 100$ ms are taken during the cryogen spurt. The boiling liquid cryogen layer and frost ring are evident in the $t = 150$ and 200 ms images. At $t = 1076$ ms, the frost layer is continuous. The white scale bar is 5-mm long.

Table 1. Summary of time required between onset of cryogen spurt (duration = τ_{cry}) and initial timepoint at which a continuous frost layer is visible (τ_{cfl}).

τ_{cry} [ms]	τ_{cfl} [ms]
20	205
40	428
60	631
80	830
100	1025

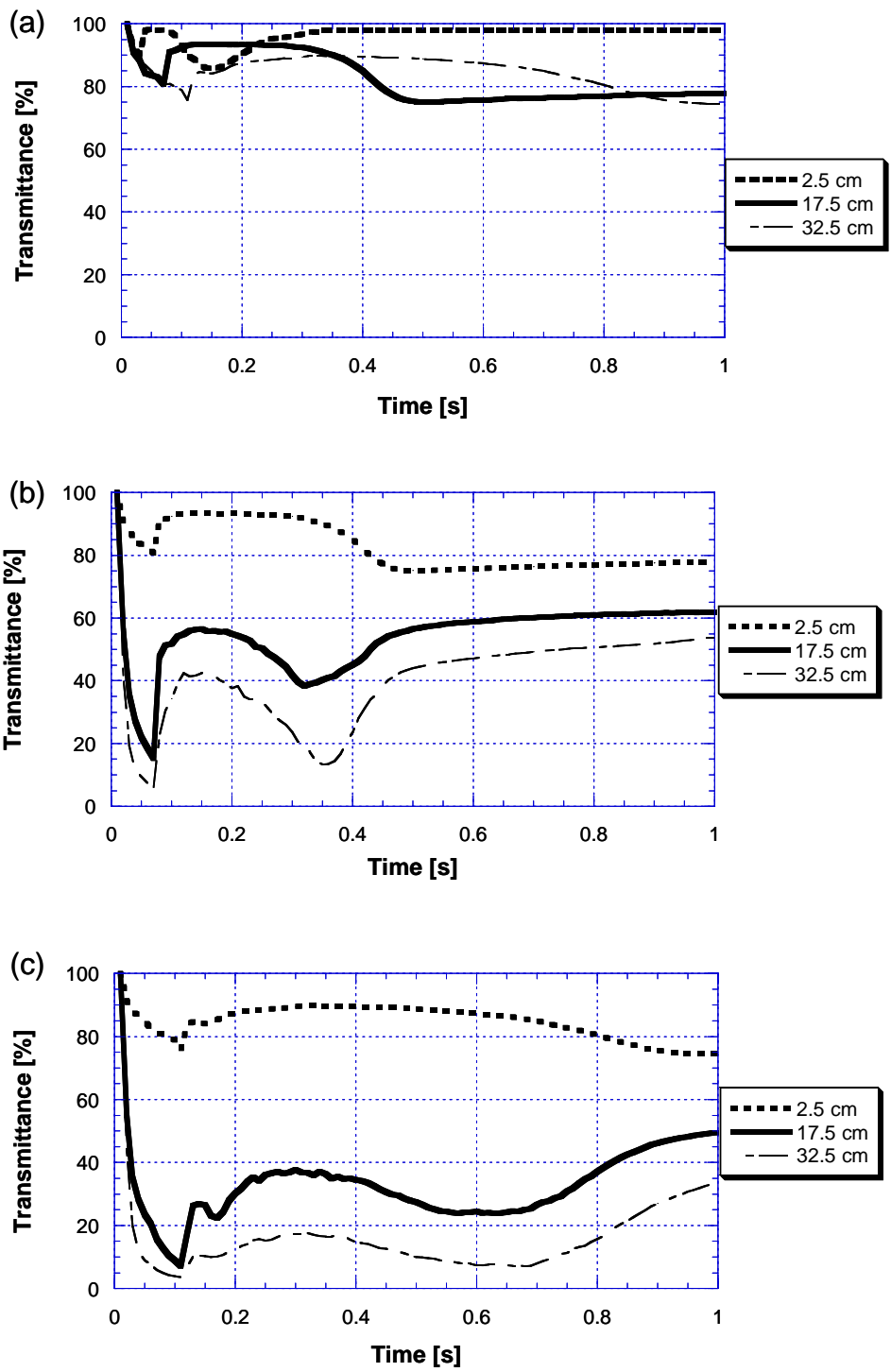


Figure 2. Time-resolved transmittance curves during CSC of glass. Cryogen spurt durations = (a) 20 ms, (b) 60 ms, and (c) 100 ms. The three curves in each plot represent transmittance measured by an apertured (1-mm-diameter) detector at three slide-detector separations d (see legend).

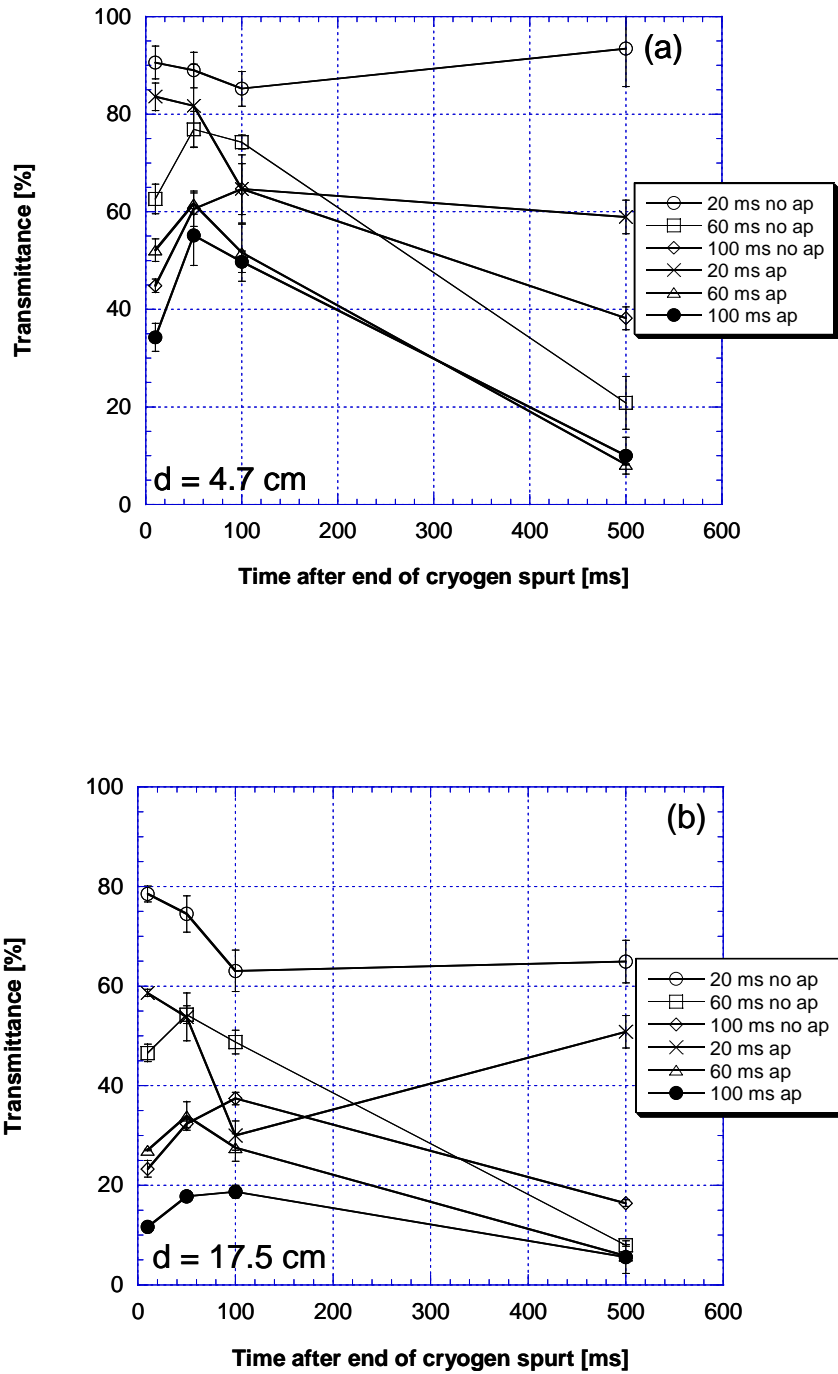


Figure 3. Transmittance values measured using pulsed laser light during cryogen spray cooling. Apertured (“ap”) and nonapertured (“no ap”) detectors were used. Two slide-detector separations [(a) 4.7 cm and (b) 17.5 cm] were investigated. The numbers in the legend correspond to cryogen spurt duration. The lines connecting the data points are shown to separate data sets and do not represent the expected time-resolved transmittance curves.

4. DISCUSSION

Ideally, the substrate used in CSC studies should be *in vivo* human skin. Unfortunately, *in vivo* light transmittance measurements are not possible due to the optical turbidity of skin at visible laser wavelengths. A limitation of using substrates such as glass (this study), aluminum [17] and copper [18, 19] is that thermal properties of these materials differ from those of human skin. Anvari et al. [20] studied heat transfer dynamics during CSC of four different materials and quantified differences in heat extraction among substrates. These results suggested that heat transfer parameters identified during CSC of one material cannot be used to provide absolute predictions of heat transfer during CSC of a different material. Nevertheless, qualitative trends can be ascertained from measurements taken during CSC of a material with considerably different thermal properties than human skin.

The pool of liquid cryogen on the glass surface was readily evident from observation of the high-speed digital images (Figure 1). When images were acquired in a previous study [21] during CSC of *in vivo* human skin, the liquid cryogen film was not readily apparent. Since the temperature and thermal diffusivity of human skin are higher than for glass, heat was transferred more rapidly to the cryogen droplets during CSC of human skin, resulting in a shorter residence time of the liquid pool. This observation is in qualitative agreement with data obtained by Choi and Welch [22] in which the residence time was an order of magnitude shorter during CSC of room-temperature gelatin tissue phantoms than for CSC of *in vivo* human skin.

Since the thermal properties of the gelatin (70% water by mass) used in Ref. 22 were expected to be similar to those of human skin, the difference in cryogen residence time suggests that substrate temperature may play a significant role in governing the overall CSC dynamics. During each light transmittance measurement, the temperature of the glass slide remained at or below room temperature. Since glass is almost perfectly transparent to visible light, the temperature of the slide is unchanged by the incident laser light. During 585-nm laser irradiation of skin, light is absorbed primarily by melanin in the epidermis and blood in the dermis, leading to an increase in local temperature. Heat diffusion from these regions towards the skin surface leads to elevated superficial temperatures and may affect the overall CSC dynamics. In particular, a temperature rise decreases the residence time of the cryogen film and frost [23]. Future studies should experimentally address the role of substrate temperature on CSC.

A preliminary integrating-sphere-based study showed that time-resolved light transmittance curves were virtually identical for four visible HeNe laser wavelengths [(543, 594, 612, and 633 nm), unpublished data]. These results suggest that cryogen film/frost layer attenuation properties are similar for light wavelengths of 585 and 594 nm. Unfortunately, the lack of wavelength-resolved cryogen optical property data makes it difficult to extrapolate the comparison to longer wavelengths such as the 755-nm and 2.94- μm light used in other studies in which transmittance was measured [13, 14].

Previous studies [24, 25] have assumed that cryogen absorption is similar to that of ice. Ice absorption coefficients at 585 nm, 755 nm, and 2.94 μm are approximately 6.8×10^{-4} , 0.01, and 11825 cm^{-1} , respectively [26]. If we assume a maximum cryogen film thickness of 6-100 μm [24, 27] and Beer's law light attenuation, the transmittance values at the three wavelengths are $\sim 100\%$, $\sim 100\%$, and $\sim 0\%$, respectively. Except for 755-nm, the measured data differ considerably from the theoretical predictions. The transmittance of 585-nm radiation at $\tau_a = 10$ ms after the end of a 100-ms cryogen spurt is 45% (Figure 3a). Majaron et al. [13] measured 80% transmittance of 2.94- μm light through a several-mm-thick liquid cryogen layer after a 2-s cryogen spurt. One possibility is that ablation of ice occurred during the laser pulse. Since the absorption coefficients of ice and water at 2.94 μm are similar [26, 28], results of skin ablation studies at 2.94 μm can provide insight into ice ablation rates. Even if ablation of cryogen occurred, skin ablation rates measured by Walsh and Deutsch [29] suggest that light transmittance would still be approximately 0%. These results suggest that the cryogen has different optical properties from ice. We are in the process of measuring collimated and diffuse reflectance and transmittance during CSC using an integrating sphere. These measurements can be used in conjunction with inverse light transport models such as the adding-doubling method [30] to calculate time-resolved effective absorption and reduced scattering coefficients of the cryogen.

CW light transmittance measurements provide a continuous record of light transmittance during CSC. Apertured light detection offers a measure of collimated light attenuation. The collimated light transmittance (T_c) trends observed for 20-ms cryogen spurts are considerably different from the 60- and 100-ms data (Figure 2). Measurements by Aguilar et al. [31] suggest that cryogen spurts shorter than 30 ms are not fully developed. Thus, the difference between the 20-ms

data and 60- and 100-ms measurements may be explained by the differences in cryogen flow characteristics and cryogen layer dynamics.

For $\tau_{\text{cry}} = 20$ ms, the transmittance curves in Figure 2a seem to be offset in time but not in decrease of T_c . For $\tau_{\text{cry}} = 60$ and 100 ms, the measurements at various d are in phase with one another but with an offset dependent on d [Figure 2(b-c)]. This is probably due to light scattering by the cryogen film/frost layer. The collection solid angle from the laser spot is different for each apertured detector position d . As d increases, the effective collection angle decreases, resulting in a decreased probability of detecting scattered light.

Pulsed 585-nm laser light detection measurements were obtained to simulate the clinical scenario as closely as possible. Although the transmittance of 585- and 594-nm radiation through the cryogen film/frost was approximately the same, the peak laser irradiance (7800 W/cm² versus 2.4×10^{-6} W/cm², respectively) differed by several orders of magnitude. If cryogen film/frost layer absorption were significant, then a difference in CSC dynamics and hence transmittance may have occurred due to direct heating of the cryogen. Preliminary measurements of pulsed laser light transmittance at different radiant exposures suggest that effects of light absorption on transmittance are negligible (unpublished data).

A direct comparison between the pulsed 585-nm and CW 594-nm data could be drawn only for apertured light detection at $d = 17.5$ cm (Figures 2 and 3b). For $\tau_d \leq 100$ ms, the 20-ms pulsed and CW T_c data differed by as much as 50%. The 60- and 100-ms pulsed and CW data agreed more closely, but discrepancies in T_c as high as 20% still existed. At $\tau_d = 500$ ms, the differences between pulsed and CW T_c data were even more pronounced. For these experiments, two DCDs were used because the measurements were taken in two different laboratories. Future experiments should focus on the use of a single cryogen delivery device for all measurements to eliminate any potential problems caused by differences between the two DCD units. Also, pulsed laser light transmittance data needs to be obtained at additional timepoints to improve the time resolution of the transmittance “curves”.

From the limited data, it is evident that T was at a local maximum at $\tau_d = 10$ ms or 50 ms (Figure 3). Typical clinical CSC parameters for PWS therapy are $\tau_{\text{cry}} = 30$ ms and $\tau_d = 30$ ms. For other dermatological procedures such as laser hair removal or nonablative skin rejuvenation, recommended $\tau_d = 10$ -80 ms. This range of τ_d appears to be appropriate, although more data points are needed and optical-thermal modeling performed to arrive at a stronger conclusion.

The time sequence of high-speed images (Figure 1) portrays the rapid changes that occur at the surface boundary of a sprayed object. The pool of cryogen liquid that forms during CSC appears to be transparent to visible light. At $t = 150$ and 200 ms after the onset of a 100-ms cryogen spurt, the glass surface is covered primarily by liquid cryogen (Figure 1). However, $T_c(d = 2.5$ cm) decreases to 85-90% at these timepoints (Figure 2c), indicating that the clear liquid film layer can attenuate incident laser light. Since an apertured detection scheme was used, the decreased T_c is due in part to scattering of light out of the reduced photodiode field of view.

At $t = \tau_{\text{en}}$ (Table 1), T_c appears to plateau for all τ_{cry} (Figure 2). Interestingly, as the annular frost ring begins to close, T_c decreases for $d = 2.5$ cm but increases for $d = 17.5$ and 32.5 cm. Intuitively, it would seem that a white (e.g., visibly-scattering) frost layer would cause an overall decrease in T_c . The reason for these trends is unknown. Simultaneous measurements of laser light transmittance and capture of high-speed images would provide a better understanding of how cryogen film dynamics affect light transmittance.

Our pulsed T_c measurements (Figure 3) involved the use of an apertured detection scheme and thus consisted primarily of collimated light transmittance. Assuming an isotropic detector, the nonapertured detector at $d = 4.7$ cm measured all light scattered at angles up to 15° with respect to the normal of the glass surface, so light scattered at larger angles was not detected. Thus, the difference between the transmittance measured in the nonapertured and apertured detection schemes provides a gross underestimate of the quantity of diffuse light scattered by the cryogen film/frost. Nevertheless, the calculated difference is as great as ~30% (Figure 3a), indicating that a considerable portion of the transmitted light consists of diffuse light. The results also suggest that the quantity of diffuse light depends on τ_{cry} and τ_d .

The practical effect of light scattering is a reduction in the quantity of collimated light and an increase in the quantity of diffuse light. Diffuse light reaching the cryogen/skin interface will either couple into the skin or reflect from the cryogen-skin interface. The effective reflectance of skin may differ for light incident at a nonzero incident angle with respect to the normal. Once light enters the skin, the angle of incidence on the skin surface is not important due to the highly scattering nature of soft tissue to visible light [32]. Since the optical properties of glass and skin differ

dramatically, it is necessary to conduct experiments involving skin or skin phantoms to understand how the data obtained in this study compare with light transport in skin.

Knowledge of the angular spread of the laser light after passage through the cryogen film and frost can lead to an improved understanding of combined CSC/laser treatment of vascular lesions such as PWS. A goniometer can be used to measure the scattering pattern of incident laser light by a sample [33]. A modified goniometric-based setup may provide experimental data on light trajectory that can be used as input into Monte Carlo models [34] to ascertain the effects of light scattering on the light distribution in skin.

5. CONCLUSIONS

In this study, time-resolved measurements of laser light attenuation during CSC were obtained. Light transmittance varied considerably during CSC. Measurements of collimated light transmittance with an apertured detection scheme suggested that light scattering by the cryogen film/frost was significant. Pulsed light detection using apertured and nonapertured detectors indicated that a substantial portion of the transmitted light was diffuse. More studies are required to ascertain the effects of light scattering by the cryogen film on laser PWS dermatologic surgery.

6. ACKNOWLEDGMENTS

The authors thank Rebecca Richards-Kortum for lending us the 594-nm HeNe laser, and John Viator and Lars Svaasand for helpful comments. This project was supported in part by research grants awarded from the National Institutes of Health (AR-43419, GM-58785, and GM-62177), the Air Force Office of Scientific Research through MURI from DDR&E (F49620-98-1-0480), the Texas Higher Education Coordinating Board (BER-ATP-253), and the Albert and Clemmie Caster Foundation. Institutional support was provided by the Office of Naval Research, National Institutes of Health and the Beckman Laser Institute and Medical Clinic Endowment.

7. REFERENCES

1. Nelson JS, Milner TE, Anvari B, Tanenbaum BS, Kimel S, Svaasand LO, and Jacques SL. Dynamic epidermal cooling during pulsed laser treatment of port-wine stain: A new methodology with preliminary clinical evaluation. *Arch Dermatol* 1995; 131:695-700.
2. Anvari B, Milner TE, Tanenbaum BS, Kimel S, Svaasand LO, and Nelson JS. Dynamic epidermal cooling in conjunction with laser treatment of port wine stains: Theoretical and preliminary clinical evaluations. *Lasers Med Sci* 1995; 10:105-112.
3. Nelson JS, Milner TE, Anvari B, Tanenbaum BS, Svaasand LO, and Kimel S. Dynamic epidermal cooling in conjunction with laser-induced photothermolysis of port wine stain blood vessels. *Lasers Surg Med* 1996; 19:224-229.
4. Torres JH, Nelson JS, Tanenbaum BS, Milner TE, Goodman DM, and Anvari B. Estimation of internal skin temperatures in response to cryogen spray cooling: Implications for laser therapy of port wine stains. *IEEE J Sel Topics Quant Elect* 1999; 5:1058-1066.
5. Waldorf HA, Alster TS, McMillan K, Kauvar ANB, Geronemus RG, and Nelson JS. Effect of dynamic cooling on 585-nm pulsed dye laser treatment of port-wine stain birthmarks. *Dermatol Surg* 1997; 23:657-662.
6. Kelly KM and Nelson JS. Update on the clinical management of port wine stains. *Lasers Med Sci* 2000; 15:220-226.
7. Chang CJ, Anvari B, and Nelson JS. Cryogen spray cooling for spatially selective photocoagulation of hemangiomas: A new methodology with preliminary clinical reports. *Plast Reconstr Surg* 1998; 102:459-463.
8. Hoffman WL, Anvari B, Said S, Tanenbaum BS, Liaw LH, Milner T, and Nelson JS. Cryogen spray cooling during Nd:YAG laser treatment of hemangiomas: A preliminary animal model study. *Dermatol Surg* 1997; 23:635-641.
9. Chang CJ, Kelly KM, and Nelson JS. Cryogen spray cooling and pulsed dye laser treatment of cutaneous hemangiomas. *Ann Plast Surg* 2001; 46:577-583.

10. Rohrer TE, Touma DJ, Ugent SJ, Goldberg LJ. Evaluating the 3-millisecond alexandrite laser with a tetrafluoroethane cooling spray for hair removal. *Arch Dermatol* (in press)
11. Lask G, Lee PK, Seyfzadeh M, Nelson JS, Milner TE, Anvari B, Dave D, Geronemus RG, Bernstein LJ, Mittelman H, Ridener LA, Coulson WF, Sand B, Baumgardner J, Hennings D, Menefee R, Berry M. Nonablative laser treatment of facial rhytides. *Proceedings SPIE* 1997; 2970:338-349.
12. Kelly KM, Nelson JS, Lask GP, Geronemus RG, Bernstein LJ. Cryogen spray cooling in combination with non-ablative laser treatment of facial rhytides. *Arch Dermatol* 1999; 135:691-694.
13. Majaron B, Kelly KM, Park HB, Verkruysse W, and Nelson JS. Er:YAG laser skin resurfacing using repetitive long-pulse exposure and cryogen spray cooling: I. Histological study. *Lasers Surg Med* 2001; 28:121-130.
14. Pope K and MacKenzie D. Analysis of attenuation by DCD. Technical Update. Wayland, MA, Candela Corporation, 2000.
15. Nelson JS, Majaron B, and Kelly KM. Active skin cooling in conjunction with laser dermatologic surgery. *Semin Cutan Med Surg* 2000; 19:253-266.
16. Khosrofian JM and Garetz BA. Measurement of a Gaussian laser beam diameter through the direct inversion of knife-edge data. *Appl Opt* 1983; 22:3406-3410.
17. Choi B and Welch AJ. Jet impingement modeling of cryogen spray cooling: Analysis of 2-D cryogen temperature distribution. *Proceedings SPIE* 2001; 4244:93-104.
18. Majaron B, Aguilar G, Basinger B, Randeberg LL, Svaasand LO, Lavernia EJ, and Nelson JS. Sequential cryogen spraying for heat flux control at the skin surface. *Proceedings SPIE* 2001; 4244:74-81.
19. Verkruysse W, Majaron B, Aguilar G, Svaasand LO, and Nelson JS. Dynamics of cryogen deposition relative to heat extraction rate during cryogen spray cooling. *Proceedings SPIE* 2000; 3907:37-48.
20. Anvari B, Pikkula BM, Tunnell JW, and Torres JH. Thermal and fluid characteristics during cryogen spray cooling. *Proceedings SPIE* 2001; 4244:105-112.
21. Choi B. Thermal Interactions of Pulsed Laser Radiation and Cryogen Spray Cooling with Skin. Ph.D. Dissertation, The University of Texas at Austin, 2001.
22. Choi B and Welch AJ. Simultaneous video and thermal imaging of cryogen spray cooling. *Proceedings SPIE* 2000; 3907:23-28.
23. Majaron B, Kimel S, Verkruysse W, Aguilar G, Pope K, Svaasand LO, Lavernia EJ, and Nelson JS. Cryogen spray cooling in laser dermatology: Effects of ambient humidity and frost formation. *Lasers Surg Med* 2001; 28:469-476.
24. Anvari B, Milner TE, Tanenbaum BS, and Nelson JS. A comparative study of human skin thermal response to sapphire contact and cryogen spray cooling. *IEEE Trans Biomed Eng* 1998; 45:934-941.
25. Anvari B, Milner TE, Tanenbaum BS, Kimel S, Svaasand LO, and Nelson JS. Selective cooling of biological tissues: Application for thermally mediated therapeutic procedures. *Phys Med Biol* 1995; 40:241-252.
26. Warren SG. Optical constants of ice from the ultraviolet to the microwave. *Appl Opt* 1984; 23:1206-1223.
27. Aguilar G, Verkruysse W, Majaron B, Svaasand LO, Lavernia EJ, Nelson JS. Measurement of heat flux and heat transfer coefficient during cryogen spray cooling for laser dermatologic surgery. *IEEE J Sel Top Quant Elect* (in press).
28. Hale GM and Query MR. Optical constants of water in the 200-nm to 200- μ m region. *Appl Opt* 1973; 12:555-563.
29. Walsh JT Jr and Deutsch TF. Er:YAG laser ablation of tissue: Measurement of ablation rates. *Lasers Surg Med* 2001; 9:327-337.
30. Prah SA, van Gemert MJC, and Welch AJ. Determining the optical properties of turbid media by using the adding-doubling method. *Appl Opt* 1993; 32:559-568.
31. Aguilar G, Majaron B, Verkruysse W, Nelson JS, and Lavernia EJ. Characterization of cryogenic spray nozzles with application to skin cooling. *Proc Int Mech Eng Cong and Exp (IMECE)* 2000; FED-V. 253:189-197.
32. Keijzer M, Jacques SL, Prah SA, and Welch AJ. Light distributions in artery tissue: Monte Carlo simulations for finite-diameter laser beams. *Lasers Surg Med* 1989; 9:148-154.
33. Jacques SL. Angular dependence of HeNe laser light scattering by human dermis. *Lasers Life Sci* 1987; 1:309-333.
34. Pfefer TJ, Barton JK, Smithies DJ, Milner TE, Nelson JS, van Gemert MJC, and Welch AJ. Modeling laser treatment of port wine stains with a computer-reconstructed biopsy. *Lasers Surg Med* 1999; 24:151-166.